This is a preprint, the final version is subject to change, of the American Mineralogist (MSA)
Cite as Authors (Year) Title. American Mineralogist, in press.
DOI: https://doi.org/10.2138/am-2019-7103

Revision 4

Solubility of Carbon and Nitrogen in a Sulfur-Bearing Iron Melt: Constraints for Iron-Loving Behavior at Upper Mantle Conditions

ALEXANDER G. SOKOL[1,2,*], ALEXANDER F. KHOKHRYAKOV[1,2], YURI M. BORZDOV[1,2], IGOR N. KUPRIYANOV[1,2], YURI N. PALYANOV[1,2]

[1]*V.S. Sobolev Institute of Geology and Mineralogy, Siberian Branch of the Russian Academy of Sciences, 3. Koptyug ave., Novosibirsk, 630090 Russia.*

[2]*Novosibirsk State University, 2. Pirogov str., Novosibirsk, 630090 Russia.*

*Corresponding author (*sokola@igm.nsc.ru)*

ABSTRACT

Carbon solubility in a liquid iron alloy containing nitrogen and sulfur has been studied experimentally in a carbon-saturated Fe-C-N-S-B system at pressures of 5.5 and 7.8 GPa, temperatures of 1450 to 1800°C, and oxygen fugacities from the IW buffer to log fO_2 ΔIW-6 (ΔIW is the logarithmic difference between experimental fO_2 and that imposed by the coexistence of iron and wüstite). Carbon saturation of Fe-rich melts at 5.5 and 7.8 GPa maintains crystallization of flaky graphite and diamond. Diamond containing 2100-2600 ppm N and 130-150 ppm B crystallizes in equilibrium with BN within the diamond stability field at 7.8 GPa and 1600°C to 1800°C, while graphite forms at other conditions. The solubility of carbon in the C-saturated metal melt free from nitrogen and sulfur is 6.2 wt.% C at 7.8 GPa and 1600°C and decreases markedly

Always consult and cite the final, published document. See http:/www.minsocam.org or GeoscienceWorld

with increasing nitrogen. A 1450-1600°C graphite-saturated iron melt with 6.2-8.8 wt.% N can dissolve: 3.6-3.9 and 1.4-2.5 wt.% C at 5.5 and 7.8 GPa, respectively. However, the melt equilibrated with boron nitride and containing 1-1.7 wt.% sulfur and 500-780 ppm boron dissolves twice less nitrogen while the solubility of carbon remains relatively high (3.8-5.2 wt.%). According to our estimates, nitrogen partitions between diamond and the iron melt rich in volatiles at $D_N^{Dm/Met}$=0.013-0.024. Pressure increase in the Fe-C-N system affects iron affinity of N and C: it increases in nitrogen but decreases in carbon. The reduction of C solubility in a Fe-rich melt containing also nitrogen and sulfur may have had important consequences in the case of imperfect equilibration between the core and the mantle during their separation in the early Earth history. The reduction of C solubility allowed C supersaturation of the liquid iron alloy and crystallization of graphite and diamond. The carbon phases could float in the segregated core liquid and contribute to the carbon budget of the overlying silicate magma ocean. Therefore, the process led to the formation of graphite and diamond which were the oldest carbon phases in silicate mantle.

INTRODUCTION

The volatiles C, N, and S have played an important role in various processes through the Earth history: early core-mantle separation, magma generation, formation of the atmosphere and minerals, etc. (Marty, 2012; Dasgupta, 2013; Shirey et al., 2013; Palyanov et al., 2013; Luth, 2014). The issues of carbon and nitrogen partitioning between the core and the mantle have received much recent attention (Marty, 2012; Dasgupta, 2013; Speelmanns et al., 2018, 2019; Grewal et al., 2019a,b). The solubility of C and N in silicate and metal melts and the respective partitioning were studied in high-pressure high-temperature experiments (Kadik et al. 2011, 2013, 2015; Roskosz et al., 2013; Dasgupta et al., 2013; Dalou et al., 2017; Speelmanns et al., 2018, 2019; Grewal et al., 2019a,b). In the experiments of Dasgupta et al. (2013) at 1-5 GPa and 1600-

Always consult and cite the final, published document. See http:/www.minsocam.org or GeoscienceWorld

2100 °C, carbon showed iron-loving behavior with partitioning between metal and silicate melts in a range of $D_C^{Met/Sil}$ = 150 to 4750; the partition coefficient increased at higher pressures but decreased at higher temperatures. Nitrogen is known to be a moderately iron-loving element at pressures from 1 to 18 GPa (Kadik et al. 2013; Roskosz et al., 2013), but its behavior in C-saturated Fe-C-N systems has been poorly understood. Roskosz et al. (2013) suggested that the solubility of nitrogen in liquid iron would not decrease much as the melt becomes saturated with carbon. Nitrogen was shown (Dalou et al., 2017) to be more soluble in the metal melt than in the silicate one ($1 \leq D_N^{Met/Sil} \leq 24$) at 1.2-3 GPa, 1400-1600°C, and fO_2 about the IW buffer, but the situation is opposite ($D_N^{Met/Sil} < 1$) in more reduced conditions. Carbon has high iron affinity in N-bearing systems at the same conditions ($100 \leq D_C^{Met/Sil} \leq 700$). As shown recently by Speelmanns et al. (2018, 2019), pressure causes strong positive influence on N solubility, increasing from 1.0 to 7.4 wt.% at 1-9 GPa (1400 °C) while temperature exerts an inverse effect at 1 GPa: N solubility decreases from 1.3 to 0.6 wt.% at 1200-1800 °C.

Judging by the high coefficient of C partitioning between silicate and metal melts in the N- and S-free system, silicate mantle should store excess carbon (Dasgupta et al., 2013), as no more than ~10–30% of the present-day mantle carbon budget can be derived from the magma ocean residual after the core-mantle separation. An explanation of the "excess" mantle carbon paradox may lie with imperfect core-mantle equilibration during the separation. In this scenario, only a small fraction (1-20%) of alloy liquid was equilibrated with a large mass of molten silicate (Dasgupta, 2013), but the local equilibration created prerequisites for C supersaturation of the melt and for graphite or diamond crystallization, i.e., carbon redistribution. In another scenario, perfect core-mantle equilibration was impossible during accretion of differentiated volatile-depleted and volatile-rich planetary embryos (Grewal et al., 2019a).

Always consult and cite the final, published document. See http:/www.minsocam.org or GeoscienceWorld

The effect of other volatiles on the solubility of carbon and nitrogen in Fe-rich liquid has been studied in the context of core-mantle equilibration since very recently (Grewal et al., 2019a,b). The fates of carbon and nitrogen during the core-mantle separation were likely interrelated (Kadik et al. 2011, 2013, 2015; Roskosz et al., 2013; Dalou et al., 2017; Grewal et al., 2019a,b). Unlike hydrogen, carbon, halogens, and most of noble gases in the Earth's silicate component which fit the chondrite model, nitrogen (1-2 ppm) is about ten times lower than the chondritic value (Marty, 2012). The deficit of nitrogen was explained (Roskosz et al., 2013) in terms of its selective redistribution in the alloy liquid and subsequent capture into the core. However, Dalou et al. (2017) concluded that carbon was selectively extracted to the metal core much more than nitrogen thus reducing the C/N ratio in the residual silicate mantle in the case of core-mantle equilibration.

The effect of sulfur on C and N partitioning between metal and silicate melts at high *P-T* conditions is another poorly investigated issue. Dasgupta et al. (2013) estimated carbon partitioning ($D_C^{Met/Sil}$) in Fe-Ni-Co-C-S systems using Fe-rich melts with 2 wt.% S. The quenched melts of S-bearing Fe-rich alloy showed modest carbon increase at graphite saturation with increasing pressure at a fixed temperature (Dasgupta et al., 2013). Grewal et al. (2019a,b) have found out that the iron affinity of carbon decreases notably in N-bearing and S-rich alloys at 1 to 7 GPa, 1500-2200°C and log fO_2 ΔIW from -4.2 to -0.8, while that of nitrogen remains largely unaffected in the presence of S. Sulfur and nitrogen may increase considerably the contribution of graphite and diamond crystallization to carbon partitioning between Fe alloy and silicate melts during imperfect core-mantle equilibration by making carbon less soluble than in the Fe-C system.

Thus, understanding the behavior of volatiles during the core-mantle separation in the magma ocean in the early Earth history requires systematic experimental research on carbon and nitrogen affinity to iron and their solubility in C-, N-, and S-bearing iron melts at upper mantle conditions. We are bridging the knowledge gap by studying the solubility of carbon and nitrogen

Always consult and cite the final, published document. See http:/www.minsocam.org or GeoscienceWorld

and crystallization of graphite and diamond in sulfur-free and sulfur-bearing iron melts at 5.5 to 7.8 GPa and 1450 to 1800°C. In order to constrain the upper limit of N which can potentially be stored in core-forming metal, the experiments were run with a Fe-based alloy containing more nitrogen than all likely building blocks involved in the Earth's accretion, given that iron meteorites contain up to 1 wt.% N (Sugiura, 1998). It is convenient to study the iron-loving behavior of C and N using N- and C-rich alloy melts.

EXPERIMENTAL AND ANALYTICAL TECHNIQUES

Starting materials

The starting compositions included chemical-grade iron nitride (Fe_3N) with 7.1 wt.% N and synthesized FeS. Sulfur concentrations in the Fe-C-N-S-B system (1.5 and 2 wt.% S) were small enough not to cause immiscibility of the metal melt within the applied pressure range (Dasgupta et al., 2009). The starting materials were stored in a vacuum desiccator at ~100 mbar and loaded in thick-walled containers before being placed into high-pressure cells, to avoid oxidation (Table 1). The containers were 2.4 mm high cylinders, 7 or 10 mm in diameter, with two or three 2.0 mm holes in each (for charging the starting materials), made of >99.99% pure graphite or chemical grade boron nitride. The containers were sealed on both sides with 0.5 mm discs of graphite or boron nitride. The boron nitride container additionally ensured good contact of the sample with graphite discs above and below. The cells were dried for at least 10 hours at 110°C between the assembly and loading into the high-pressure apparatus.

High-pressure apparatus

Always consult and cite the final, published document. See http:/www.minsocam.org or GeoscienceWorld

Experiments at 5.5 and 7.8 GPa were carried out in a split-sphere multi-anvil high-pressure apparatus (Palyanov et al. 2010). Sizes of pressure cells were 21.1×21.1×25.4 mm and 19×19×22 mm, respectively, in the 5.5 and 7.8 GPa runs; graphite heaters in the two pressure runs had an inner diameter of 12 mm and 9 mm and a height of 18.8 mm and 14.8 mm, respectively. Pressure was calibrated by recording the change in the resistance of Bi at 2.55 GPa and PbSe at 4.0 and 6.8 GPa at room temperature and at 1350°C by bracketing the graphite-diamond equilibrium in the $Ni_{0.7}$-$Fe_{0.3}$-C system. Temperature was monitored in each experiment with a $PtRh_6/PtRh_{30}$ thermocouple calibrated at 6.3 GPa using the melting points of Al, Ag (Palyanov et al., 2010; Sokol et al., 2015). Pressure and temperature were measured to an accuracy of ± 0.1 GPa and ± 40°C, respectively (Palyanov et al., 2010; Sokol et al., 2015).

Analytical methods

The recovered run products were cleaned, dried and cut into halves (longitudinally, to produce a full top-to-bottom section) and then one half was mounted in epoxy resin by vacuum impregnation. After resin polymerization, the samples were polished under kerosene, without the use of water (final stage 1 μm Al_2O_3) and examined on a *Tescan MIRA 3 LMU* scanning electron microscope (SEM) and under a *Carl Zeiss Stemi 2000-C* optical microscope. For preliminary semi-quantitative determination, their compositions were analyzed on the *Tescan MIRA 3 LMU* scanning electron microscope coupled with an INCA EDS 450 microanalysis system with an Oxford Instruments liquid nitrogen-free large area *EDS X-Max-80* Silicon Drift Detector. The instruments were operated at an accelerating voltage of 20 keV, a beam current of 1 nA, and a spot diameter of ~ 10 nm; the count time for spectra collection was 20 s. The EDS spectra were optimized for quantification using the standard XPP procedure built into the *INCA Energy 450* software.

Always consult and cite the final, published document. See http:/www.minsocam.org or GeoscienceWorld

The C, N and S concentrations were determined quantitatively on *a Carlo Erba-1106 CHN and Euro EA 3000 CHNS analyzers*. Analyses were applied to selected pieces from the central parts of the quenched samples, which contained soot-like carbon but were free from newly formed graphite. Then 0.5-2.0 mg aliquots (two for each sample) placed in tin capsules and pre-weighed on a *Sartorius CP2P* balance were oxidized in a He stream doped with 10 ml O_2 in a vertical reactor at 1050°C, in a dynamic mode. After complete oxidation, the CO_2, H_2O and nitrogen oxides passed through a reduction zone, where hot copper removed excess oxygen and reduced nitrogen oxidized to N_2. In the EA analyzer, the mixture of sulfur oxides was quantitatively converted to SO_2 on reduced copper. The resulting N_2, CO_2, SO_2 and H_2O mixture was separated in a *Porapak Q* column, and individual eluted gases were measured with a thermal conductivity detector to an accuracy of ±0.3 wt. %. Two values obtained for each sample were averaged. The details of the method were reported previously by Fadeeva et al. (2008).

Additionally, element abundances in the quenched liquids were determined by electron microprobe analysis (EPMA) on a *Jeol JXA-8100* microanalyzer at 15 kV accelerating voltage, 200 nA beam current, and 30 μm beam diameters, at 10 nm chromium sputtering. The results were checked against Fe_3N, Fe_3C, Fe^0 and FeS_2 standards. The measured intensities were converted to concentrations by the ZAF method. The C and N contents in solid phases were estimated to an error of 5 rel.%, the Fe and S contents were accurate to 2 rel.%, and the accuracy decreased to 10 rel.% error in the case of low C, N, and S concentrations in the samples. The detection limit for C, N, and O was ~0.1 wt.% at the applied analytical conditions.

Measuring C and N contents in quenched melt samples after high-pressure high-temperature runs is problematic (Dasgupta et al., 2013; Dalou et al., 2017; Sokol et al., 2017). Problems arise with electron microprobe analysis (EPMA), as well as with defocused beam scanning of melts containing randomly distributed C- or N-rich dendritic crystals up to 0.5 mm long (Sokol et al., 2017). The impact of this factor was estimated by comparing the compositions

Always consult and cite the final, published document. See http:/www.minsocam.org or GeoscienceWorld

of quenched melts determined by *a Carlo Erba-1106 CHN* and *Euro EA 3000 CHNS* analyzers and a *Jeol JXA-8100* microanalyzer. The C and N concentrations obtained by different methods were in reasonable agreement (Table 1; Supplementary Table 2 and Supplementary Figure 1), but S showed a surprisingly large misfit (Supplementary Fig. 2): the EMPA values, especially at <1.5 wt.% S, were 25-50% lower than those of *Euro EA 3000 CHNS*. The misfit most likely resulted from uneven distribution of S-rich lamelli (Fig. 3). On the other hand, the size and position of C- and N- enriched dendrites were suitable for EPMA estimation. In general, the reported element concentrations were mainly determined with the *Carlo Erba-1106 CHN* and *Euro EA 3000 CHNS* analyzers.

The concentrations of boron were determined on a ThermoJarrell Intertech *IRIS Advantage* atomic-emission mass spectrometer (USA). The samples were decomposed using alkali fusion with a KOH flux. 2.5 to 8.6 mg specimens of were placed in glass-carbon crucibles and heated gradually from room temperature to 550 °C for two hours with NaOH and 40-60 mg KOH per dry weight. As the system reached the design temperature, the crucibles were cooled down, then 1 ml H_2O were added, the melt was digested in 1 ml of 6 M HCl, and the solution was poured into a 5 ml vial. The B contents were calculated using external calibration, with Sc as an internal standard. According to a test run, the analytical materials (vials and reagents) used for boron determination were pure within 1.5 rel.%. The B content in the metal alloy was accurate to 10 rel.%.

The quench melt phases were identified by X-ray powder diffraction on a *Stoe IPDS-2T* diffractometer (MoKα radiation, graphite monochromator) in the Gandolfi mode. Two-dimensional X-ray patterns were radially integrated using the XArea software package. The diffraction profiles were processed in *WinXPow (Stoe)*. The database of PDF-4 Minerals (The Powder Diffraction File PDF-4 +, 2006) was used for phase analysis.

Diamond crystals produced in several runs were studied by Fourier transform infrared (FTIR) absorption micro-spectroscopy. The recovered diamonds were cleaned in a hot mixture of

Always consult and cite the final, published document. See http:/www.minsocam.org or GeoscienceWorld

concentrated H_2SO_4 and 30% water solution of $K_2Cr_2O_7$ and then fixed in a perforated indium foil. The FTIR spectra were acquired using a *Bruker Vertex 70 FTIR* spectrometer coupled with a *Hyperion 2000* microscope, with a resolution of 2 cm^{-1} and averaging over 64 scans, using 50 to 100 μm square apertures depending on sample size.

RESULTS

Scanning electron microscopy of polished samples that represented the Fe-C-N and Fe-C-N-S-B systems revealed a particular texture produced by dendritic crystals (Fig. 1a-c), which apparently resulted from quenching of the obtained Fe-rich melt. The Fe-C-N samples consisted of C-rich dendritic crystals with an N-rich metal phase and interstitial wüstite (FeO). The needle-like C-rich dendritic crystals of the Fe-C-N-S-B samples contained notably larger amounts of interstitial quench iron nitride, more depleted in nitrogen than that of the Fe-C-N system. The Fe-C-N-S-B samples also enclosed elongate drop-shaped 1 to 10 μm S-bearing metal particles.

According to the X-ray powder diffraction analysis of the quenched liquid, the Fe-C-N-S-B samples contained iron nitride, iron carbide (Fe_3C), high-temperature γ-Fe, soot-like carbon, and pyrrhotite. Thus, the quenching produced host phases capable of accumulating carbon, nitrogen, and sulfur and holding them back in the samples. The metal melt did not lose C, N and S during quenching, and the fragments of quenched samples can be expected to store record of the C, N and S contents. This inference agrees with published evidence (Dasgupta et al., 2013; Roskosz et al., 2013; Dalou et al., 2017).

The presence of FeO segregations in the Fe-C-N quenched samples indicates an oxygen fugacity about the IW buffer. The runs with the Fe-C-N-S-B system were performed using containers made of boron nitride which can impose exceedingly low fO_2 values, via the

Always consult and cite the final, published document. See http:/www.minsocam.org or GeoscienceWorld

equilibrium $4BN+3O_2=2B_2O_3+2N_2$. Proceeding from the compositions of the metal and silicate (almost FeO-free) melts in BN capsules equilibrated at 1.5 GPa and 1600-1900°C, Ballhaus et al. (2013) concluded that the samples were as reduced as log fO_2 ΔIW-6. This low value is consistent with the absence of FeO segregations in the quenched samples.

Iron nitride used as a starting material contained 7.1 wt.% N. Nitrogen became less soluble as the nitride melt dissolved also carbon and sulfur, and excess N released into the fluid phase remained partly preserved in graphite pores (Speelmanns et al., 2018) and partly escaped from the system through the leaking capsules. The fluid phase in equilibrium with C and N-bearing iron melt consisted mainly of NH_3, N_2, H_2O and light alkanes (Sokol et al., 2018). The dissolution of carbon in the Fe-C-N system led to its respective saturation and crystallization of graphite (Fig. 1d), while the concentration of nitrogen remained about the starting level (Table 1; Fig. 2a). The excess over starting N concentrations in some samples may be due to partial oxidation of iron. At 1450 to 1600°C, the melt, contained only 3.6-3.9 and 1.4-2.5 wt.% C at 5.5 and 7.8 GPa, respectively (Fig. 2b). On the other hand, the 6.2 wt.% carbon solubility in a nitrogen-free C-saturated iron melt obtained at 7.8 GPa and 1600°C is in line with the results of Lord et al. (2009).

The effect of low N concentrations on carbon solubility in the Fe-rich melt has been beyond this study but it was tested previously for the Fe-C-N system at 7.8 GPa and 1350°C (Sokol et al., 2017). Nitrogen increase from 0.3 to 3.8 wt.% at 1350°C was found out to reduce carbon solubility from 4.8 wt.% in a C-saturated iron melt equilibrated with iron carbide (Fe_3C) and graphite to 2.3 wt.% in that equilibrated with iron nitride (ε-Fe_3N) and graphite (Fig. 4).

The presence of 1.5-2.1 wt.% S in alloy melt in equilibrium with graphite, at 5.5 GPa, 1600°C and fO_2 ~IW, led to nitrogen decrease from 7.1 to 5.3-5.4 wt.% (Table 1), while carbon was 3.5-3.6 wt.%. The presence of 0.9-1.7 wt.% S and 500-780 ppm B in the alloy melt equilibrated with graphite and BN, at 1600°C and ~log fO_2 ΔIW-6, led to nitrogen decrease from 7.1 to about 4.5

Always consult and cite the final, published document. See http:/www.minsocam.org or GeoscienceWorld

wt.% at both 5.5 and 7.8 GPa (Fig. 3). The nitrogen concentrations showed a greater variance at 1800°C, but the average values likewise approached 4.5 wt.% N (Table 1). The solubility of carbon in a C-saturated melt in the same system, within the applied *P-T-f*O_2 range, was about 4.5 wt.% on average and remained around 3.8-3.9 wt.% C only at 5.5 GPa and 1600°C. In the presence of sulfur, carbon became almost twice more soluble in an N-rich iron melt at 7.8 GPa and 1600°C (4.6-4.7 wt.% against 1.4-2.5 wt.% for the Fe-C-N system). Minor S variations did not change notably the concentrations of C and N in the quenched melt.

The samples became saturated with carbon upon their contact either with the walls of the graphite container (Fe-C-N system) or with the graphite discs on the ends (Fe-C-N-S-B system) under the applied *P-T* conditions. The saturation became evident as newly formed graphite flakes appeared at the contact with the container at the conditions of graphite (5.5 GPa; 1600 and 1800°C) and diamond (7.8 GPa; 1600°C) stability. Graphite formed within the stability fields of both graphite and diamond because diamond formation in an N-rich C-saturated iron melt is kinetically hindered at the respective pressures and temperatures (Borzdov et al., 2002). In 7.8 GPa and 1600°C runs with the Fe-C-N-S-B system, diamond formed by the mechanism of film growth (FG) in the graphite source (Pal'yanov et al., 2001; Palyanov and Sokol, 2009). In 1-hr runs at 1600°C, about 60-70% of graphite converted to diamond which appeared as aggregates of dark green to black octahedral and twin crystals reaching 200 μm in size (Fig 5a). At a higher temperature of 1800°C, already 90-95% of graphite converted to diamond in 30 minutes; the diamond crystals occurred as ≤1 mm dark green octahedra (Fig. 5b) or often as contact or cyclic twins (Fig. 5c), with numerous BN tetrahedra aligned with the diamond {111} faces on the surfaces (Fig. 5d). In another run, the whole graphite pellet converted to diamond looking like an aggregate of pale green and colorless grains.

Given rather specific conditions of diamond crystallization with the system composition rich in both nitrogen and boron, it is of particular interest to study impurities in the synthesized

Always consult and cite the final, published document. See http:/www.minsocam.org or GeoscienceWorld

diamonds, especially nitrogen and boron known to be the main ones. The type and concentration of the corresponding defects can be assessed from FTIR spectra, like that of Fig. 6 for diamond crystals synthesized at 1600°C (run 2106_2_2). Note that reasonably good quality of FTIR spectra was achieved only for a few transparent thin {111} cleavage plates of diamond because most of the diamonds synthesized in that run were irregular aggregates which yielded considerably distorted spectra with interference fringes. The spectrum of Fig. 6 shows strong absorption bands of nitrogen impurities in the defect-induced one-phonon region (1400-800 cm^{-1}) but no features related to boron impurities. The one-phonon spectrum consists of bands produced by single substitutional nitrogen atoms, or C centers (peaking at 1130 cm^{-1}), and pairs of nearest-neighbor nitrogen atoms, or A centers (peaking at 1280 cm^{-1}). The N concentrations were calculated using the recorded spectra normalized to the thickness of samples which was estimated using an optical microscope with a motorized XYZ-stage. The thickness estimation was quite reasonable, judging by a reference FTIR spectrum of type IIa diamond shown in Fig. 6 for comparison. The concentrations of C- and A-form nitrogen were determined by decomposing the FTIR spectra, in the one-phonon region, into A and C components and using conversion factors of 16.5 atomic ppm cm^{-1} of absorption at 1280 cm^{-1} for the A centers (Boyd et al., 1994) and 25 atomic ppm cm^{-1} of absorption at 1130 cm^{-1} for the C centers (Kiflawi et al., 1994). For the spectrum of Fig. 6, they were approximately 1600-1800 ppm for C-form nitrogen and 700-800 ppm for A-form nitrogen, or 2300-2600 ppm in total. The uncertainty in the calculations was due to spectrum distortion and errors in sample thicknesses.

Diamond crystals synthesized at 1800°C (runs 623_8_1 and 623_8_2) generally had larger sizes and better quality. Therefore, it was possible to acquire relatively little distorted FTIR spectra for both individual diamond crystals or blocks and fragments of fractured diamond aggregates. Typical spectra in Fig. 7 show strong signals in the one-phonon region, mostly due to the A-form nitrogen. The bands of C-centers are either much weaker or undetectable, possibly, because of

Always consult and cite the final, published document. See http:/www.minsocam.org or GeoscienceWorld

annealing effects at a higher temperature of synthesis. The FTIR spectra of diamonds synthesized at the same temperature but with slightly different starting compositions were similar. The recorded FTIR spectra were converted to the absorption coefficient by fitting to the standard spectrum of type IIa diamond in order to obtain the best fit of intrinsic two-phonon bands (2700-1700 cm^{-1}). The calculated nitrogen concentrations were within 2100-2400 ppm, i.e., they did not differ much from those found for diamonds synthesized at 1600 °C. Note that the spectra of some diamond samples contained features (a sharp peak at 1332 cm^{-1} and broader bands at 1050 cm^{-1} and 950 cm^{-1}, inset in Fig. 7) due to positively charged single substitutional nitrogen (N^+-centers), besides the A- and C-centers. The presence of N^+-centers most probably results from the incorporation of boron in the crystal structure. Single substitutional nitrogen and boron atoms in diamonds are known to act as donor and acceptor centers, respectively, so N^+ and B^- centers should arise for charge balance. At the time being, no information is available on the presence of B^- centers in diamond FTIR spectra, but their concentration can be assumed to be approximately equal to that of N^+ centers. As calculated using known calibrations (Lawson et al., 1998), the diamond sample presented in panel *a* of Fig. 7 may contain about 130-150 ppm of N^+ centers and about the same amount of B^- centers. These values do not affect much the overall N concentration for the analyzed diamonds and indicate that the growing crystals accommodated more nitrogen than boron.

Although the estimated N contents in diamond are slightly lower than the highest values found so far (e.g., 3000-3300 ppm for diamonds synthesized in the Fe_3N-C system (Borzdov et al., 2002)), they still are at the upper bound achieved to date by using various N-enriched diamond growth systems (Zhang et al., 2008; Yu et al., 2008; Palyanov et al., 2010; Sun et al., 2014).

DISCUSSION

Always consult and cite the final, published document. See http:/www.minsocam.org or GeoscienceWorld

The obtained data reveal main trends in the solubility of carbon and nitrogen in a sulfur-free and sulfur-bearing iron melt at upper mantle conditions. The content of carbon in a metal melt equilibrated with graphite decreases from 4 wt.% at 0.1 MPa (Bouchard and Bale, 1995) to about 2.0 wt.% at 7.8 GPa in an N-rich iron melt. At 7.8 GPa and 1400-1600°C, the solubility of carbon in this melt is weakly sensitive to temperature (Fig. 2b). Nitrogen saturation of the melt is evident from comparison of N concentrations in samples of molten Fe_3N in graphite containers with those in melts equilibrated with N_2 fluids (Fig. 2) (Speelmanns et al., 2018). Excess nitrogen in the samples apparently formed at the account of partial Fe oxidation. Thus, our results, compared with previously reported data (Bouchard and Bale, 1995; Roskosz et al., 2013; Dalou et al., 2017; Speelmanns et al., 2019), show that nitrogen solubility in 1600°C C-saturated iron alloy liquid increases with pressure. The concentration of nitrogen in a C-saturated S-free liquid formed by melting of Fe_3N increases from 0.045 wt.% N at P_{N2}=0.1 MPa to about 7.3 wt.% N at 7.8 GPa (Fig. 8). Note that nitrogen solubility was reported to decrease with increasing temperature at 1 GPa (Speelmanns et al., 2018), but we observed nitrogen increase in a C-saturated Fe-C-N melt as the temperature increased from 1400 to 1600°C at 5.5-7.8 GPa (Fig. 2a), and some N contents at 1600°C (Fig. 8) were even above the calculated N solubility limit of Speelmanns et al. (2018).

The C-saturated Fe_3N melt equilibrated with BN contained from 30% (at 5.5 GPa) to 50% (at 7.8 GPa) less nitrogen in the presence of 0.9-1.7 wt.% S than without sulfur. Importantly, even minor concentrations of sulfur can increase carbon solubility in N-rich Fe alloy melts: the carbon concentration in C-saturated and S-free Fe_3N melt is from 2.3-2.4 wt.% C at 7.8 GPa and 1600°C but reaches 4.6-4.7 wt.% C in the presence of 1.1 wt.% S in the same melt (Fig. 9a). The similarity of C and N concentrations in S-bearing quenched melts, after runs in graphite and BN containers (Fig. 9a,b), indicates that fO_2 does not affect much the solubility of C and N in Fe-based alloy melts. Diamonds synthesized in some runs with BN containers had BN crystals on the surface (Fig. 5c,d), which precipitated from the B- and N-bearing melt. However, B concentrations in the

Always consult and cite the final, published document. See http:/www.minsocam.org or GeoscienceWorld

quenched melts were 500-780 ppm. Therefore, the solubility of C and N in Fe-based melts is insensitive to the presence of B impurity and changed in our case only because the melt contained 1-2 wt.% S. Note that N solubility in the presence of S approaches that for an S-free melt at a lower pressure of 2-3 GPa (Dalou et al., 2017) (Fig. 2).

In this experimental study we have confined ourselves to a single aspect of carbon and nitrogen behavior during the metal-silicate separation in the magma ocean: the solubility of C and N in metal melts at different conditions and starting compositions. As demonstrated by the available data, even minor concentrations of nitrogen can lead to marked decrease in carbon solubility in the iron melt at 7.8 GPa and 1350°C (Fig. 4) (Sokol et al., 2017). The experiments with the Fe-C-N system at a higher pressure than in those of Dalou et al. (2017) show greater solubility of nitrogen in the metal melt but lower carbon solubility, i.e., nitrogen acquires a greater iron affinity than carbon as pressure increases. This confirms the inference by Speelmanns et al. (2018) and Grewal et al., (2019a) that the iron affinity of C in Fe-based alloys becomes lower than that of N at increasing pressure. The presence of sulfur can reduce the solubility of N and C in Fe-C-N-S melts. The solubility of nitrogen and carbon in a melt containing 1 to 2 wt.% S was 30 % (N) and 50% (C) lower than in a pure iron liquid (Table 1, Fig. 9). Thus, according to our data, the iron affinities of C and N become commensurate at 5.5-7.8 GPa and 1600-1800°C, in the presence of minor sulfur. If the sulfur content exceeds 10 wt.%, it can reduce the iron affinity of carbon, while the iron-loving behavior of nitrogen remains at the same level (Grewal et al., 2019a,b).

The fate of C and N during the core-mantle separation was determined by their partitioning between metal and silicate melts. Recent results (Dalou et al. 2017; Speelmanns et al. 2019; Grewal et al. 2019a,b) provide explicit evidence that C is more siderophile than N at almost any *P*-*T*-fO_2 conditions of the core formation, i.e. $D_C^{Met/Sil} > D_N^{Met/Sil}$. The revealed trends of C and N solubility in iron melts have contributed to $D_C^{Met/Sil}$ and $D_N^{Met/Sil}$ variations, but they do not change the siderophile behavior of carbon and the lithophile behavior of nitrogen in the process.

Always consult and cite the final, published document. See http:/www.minsocam.org or GeoscienceWorld

The coefficient $D_N^{Met/Sil}$ can exceed $D_C^{Met/Sil}$ only in the case of extremely high S contents (Grewal et al. 2019a). The fact that nitrogen can become more soluble in the metal melts than carbon with increasing pressure suggests that some N might be segregated to the core. However, the scale of the processes is difficult to assess, thus more data are necessary to understand of the causes of the high C/N ratio in the bulk silicate Earth.

During the separation between the core and the mantle in the case of their imperfect equilibration, low carbon solubility in an N- and S-bearing iron melt could play an important role in the fate of both carbon and nitrogen: it increased the probability for local C supersaturation of the liquid alloy and the ensuing crystallization of graphite and diamond. Newly formed carbon phases could float in the segregating core liquid and contribute to the overlying silicate magma ocean carbon budget. Further fate of carbon was likely controlled by the density ratio of silicate magma (2700 kg/m^3 for peridotite melt at 0.1 MPa and 2000 K (Courtial et al., 1997) and ~3500 kg/m^3 at 15 GPa and 2200-2500°C (Ohtani and Maeda, 2001)), diamond (3530 kg/m^3 at ambient *P-T* conditions), and graphite (2100-2250 kg/m^3 at ambient *P-T* conditions). Graphite could float and then be dynamically stable at the surface of a reduced magma ocean (Keppler and Golabek, 2019). As estimated in the first approximation (without regard to the size grains and to the life span of magma ocean), diamond at depths corresponding to its thermodynamic stability could be suspended in the magma ocean. After cooling and crystallization of the silicate melt, it could concentrate near the level where the silicate melt and diamond had similar density.

The segregation of the solid metal phase at a lower temperature implies participation of a fluid phase, which was totally dissolved in silicate melt at temperatures higher than the liquidus for silicate mantle. As shown previously (Sokol et al., 2018), nitrogen at 6.3-7.8 GPa and 1200-1400°C has greater iron affinity in the metal-fluid partitioning than carbon: $D_N^{Met/Fl}$>$D_C^{Met/Fl}$. In this case, carbon (as hydrocarbons) and nitrogen (to a lesser degree, as N_2 and NH_3) will be stable

Always consult and cite the final, published document. See http:/www.minsocam.org or GeoscienceWorld

in the fluid at the upper mantle pressures, and the fluid can further transport the volatiles to the Earth's surface.

The data on N contents in iron liquid alloy (molten Fe_3N) and in diamond that crystallized from this melt at 7.8 GPa and 1600 and 1800°C, have provided the first constraints on melt-diamond nitrogen partitioning. Diamond with 2100-2600 ppm N crystallized from an S-bearing, Fe-rich melt that contained 101,000 to 163,000 ppm N (10.1-16.3 at.%), i.e., $D_N^{Dm/Met}$= 0.013-0.024. The low partition coefficient confirms the conclusion on relative incompatibility of N in diamonds compared with metallic Fe (Smith and Kopylova, 2014). This value is consistent with our earlier results (Borzdov et al., 2002) obtained at 7.0 GPa and 1700-1850°C in experiments of diamond growth on seeds in a C-saturated Fe_3N liquid which yielded diamond with ~3300 ppm N. The low $D_N^{Dm/Met}$value indicates that diamond crystallization and subsequent floating in the metal melt should not cause considerable N escape from the segregating core liquid to the overlying silicate magma.

The $D_N^{Dm/Met}$value we obtained is markedly higher than that ($D_N^{Dm/Met}$=0.0005) estimated from data on lower mantle diamond from Juina, Brazil, with 44 ppm N, which contains inclusions of Fe-carbides with 73,000–91,000 ppm N (Kaminsky and Wirth, 2011). The pressure increase from 7-8 GPa to typical lower mantle pressures may lead to additional increase of N solubility in the metal melt (Roskosz et al. 2013) and to lower $D_N^{Dm/Met}$ (Smith and Kopylova, 2014). Comparison with the available data indicates that sulfur can interfere with diamond crystallization and influence on nitrogen partitioning between diamond and liquid alloy. Diamond crystals synthesized in the nominally N-free $(Fe,Ni)_9S_8$–C system were found to contain nitrogen impurity with concentrations of an order of 1000 ppm (Palyanov et al., 2006). Therefore, $D_N^{Dm/Met}$ in an S-rich melt is much higher $D_N^{Dm/Met}$= 0.013-0.024 than that inferred for an N-rich melt with 1-2

Always consult and cite the final, published document. See http:/www.minsocam.org or GeoscienceWorld

wt.% S. Thus, the Juina lower mantle diamond and some of N-free sublithospheric diamonds (Smith and Kopylova, 2014; Smith et al., 2016) may have grown in an S-poor environment.

IMPLICATIONS

Partitioning between a Fe-rich alloy and silicate magma influenced greatly the fates of C, N, S and other volatiles during the core-mantle separation early in the Earth's history. Experimental studies of the solubilities of volatiles in Fe-rich alloy melts and in silicate magma can provide insights into the causes of nitrogen "deficit" and carbon "excess" in the mantle, which is currently among major theoretical challenges. The results of this work, compared with earlier published data, show that iron affinity of carbon decreases while that of nitrogen increases as pressure increases from 1.2 to 7.8 GPa. The iron-loving behavior shows up in more than two-fold decrease of carbon solubility in an N-rich graphite-saturated iron melt. On the other hand, the solubilities of C and N become commensurate in a melt containing 1-1.7 wt.% S. The $D_N^{Dm/Met}$=0.013-0.024 partitioning of nitrogen between diamond and a nitrogen- and sulfur-bearing Fe-rich alloy liquid indicates greater incompatibility of N in diamond than in iron melts. In the case of the imperfect core-mantle equilibration scenario, even minor concentrations of volatiles would create prerequisites for C supersaturation of Fe-rich alloy and the ensuing crystallization of graphite and diamond. Later on graphite and diamond could float from the segregated core liquid and contribute to the carbon budget of the overlying silicate magma ocean. Such graphite and diamond that were present in the forming silicate mantle were likely the oldest carbon phases.

ACKNOWLEDGMENTS

Always consult and cite the final, published document. See http:/www.minsocam.org or GeoscienceWorld

We wish to thank Alexey Kruk, Elena Nigmatulina and Olga Kozmenko for assistance throughout the study. The SEM, EPMA and AES analytical work was carried out at the Analytical Center for Multi-Elemental and Isotope Research (Novosibirsk). The manuscript profited much from thoughtful reviews by Celia Dalou and an anonymous reviewer. The study was supported by grant 16-17-10041 from the Russian Science Foundation. Experiments with the Fe-C-N-S system were performed as part of a government assignment to the V.S. Sobolev Institute of Geology and Mineralogy (Novosibirsk).

REFERENCES CITED

Ballhaus, C., Laurenz, V., Münker, C., Fonseca, R.O., Albarède, F., Rohrbach, A., Lagos M., Schmidt M.W., Jochum K.-P., Stoll B., Weis, U., and Helmy H.M. (2013) The U/Pb ratio of the Earth's mantle - A signature of late volatile addition. Earth and Planetary Science Letters, 362, 237-245.

Borzdov, Y., Pal'yanov, Y., Kupriyanov, I., Gusev, V., Khokhryakov, A., Sokol, A., Efremov, A. (2002) HPHT synthesis of diamond with high nitrogen content from an Fe_3N–C system. Diamond and Related Materials, 11, 1863-187.

Bouchard, D., and Bale, C.W. (1995) Simultaneous optimization of thermochemical data for liquid iron alloys containing C, N, Ti, Si, Mn, S and P. Metallurgical and Materials Transactions B 26B, 467–484.

Boyd, S.R., Kiflawi, I., and Woods, G.S. (1994) The relationship between infrared absorption and the A defect concentration in diamond. Philosophical Magazine, B 69, 1149-1153.

Courtial, P., Ohtani, E. Dingwell, D.B. (1997) High-temperature densities of some mantle melts. Geochimica et Cosmochimica Acta 61, 3111–3119.

Always consult and cite the final, published document. See http:/www.minsocam.org or GeoscienceWorld

Dalou, C., Hirschmann, M.M., von der Handt, A., Mosenfelder, J., and Armstrong, L.S. (2017) Nitrogen and carbon fractionation during core–mantle differentiation at shallow depth. Earth and Planetary Science Letters, 458, 141–151.

Dasgupta, R., Buono, A., Whelan, G., and Walker, D. (2009) High pressure melting relations in Fe–C–S systems: implications for formation, evolution, and structure of metallic cores in planetary bodies. Geochimica et Cosmochimica Acta, 73, 6678–6691.

Dasgupta, R. (2013) Ingassing, storage, and outgassing of terrestrial carbon through geologic time. Reviews in Mineralogy and Geochemistry, 75(1), 183-229.

Dasgupta, R., Chi, H., Shimizu, N., Buono, A.S., and Walker, D. (2013) Carbon solution and partitioning between metallic and silicate melts in a shallow magma ocean: implications for the origin and distribution of terrestrial carbon. Geochimica et Cosmochimica Acta, 102, 191–212.

Fadeeva, V.P., Tikhova, V.D., and Nikulicheva O.N. (2008) Elemental Analysis of Organic Compounds with the Use of Automated CHNS Analyzers. Journal of Analytical Chemistry 63, 1094–1106.

Grewal, D.S., Dasgupta, R., Sun, C., Tsuno, K., and Costin, G. (2019a). Delivery of carbon, nitrogen, and sulfur to the silicate Earth by a giant impact. Science advances 5(1), eaau3669.

Grewal, D.S., Dasgupta, R., Holmes, A.K., Costin, G., Li, Y., and Tsuno, K. (2019b). The fate of nitrogen during core-mantle separation on Earth. Geochimica et Cosmochimica Acta 251, 87-115.

Kadik A.A., Kurovskaya N.A., Ignat'ev Yu.A., Kononkova N.N., Koltashev V.V. and Plotnichenko V.G. (2011) Influence of oxygen fugacity on the solubility of nitrogen, carbon, and hydrogen in $FeO–Na_2O–SiO_2–Al_2O_3$ melts in equilibrium with metallic iron at 1.5 GPa and 1400°C. Geochemistry International, 49, 429-438.

Always consult and cite the final, published document. See http:/www.minsocam.org or GeoscienceWorld

Kadik, A. Litvin, Y.A., Koltashev, V.V., Kryukova, E.B., Plotnichenko, V.G., Tsekhonya, T.I., and Kononkova, N.N. (2013) Solution behaviour of reduced N–H–O volatiles in FeO–Na_2O–SiO_2–Al_2O_3 melt equilibrated with molten Fe alloy at high pressure and temperature. Earth and Planetary Science Letters, 214, 14-24.

Kadik, A.A., Koltashev, V.V., Kryukova, E.B., Plotnichenko, V.G., Tsekhonya, T. I., and Kononkova, N.N. (2015) Solubility of nitrogen, carbon, and hydrogen in FeO–Na_2O–Al_2O_3–SiO_2 melt and liquid iron alloy: influence of oxygen fugacity. Geochemistry International, 53(10), 849-868.

Keppler, H., and Golabek, G. (2019). Graphite floatation on a magma ocean and the fate of carbon during core formation. Geochemical Perspectives Letters, 11, 12-17.

Kaminsky, F.V., Wirth, R., (2011) Iron carbide inclusions in lower-mantle diamond from Juina, Brazil. Canadian Mineralogist, 49, 555–572.

Kiflawi, I., Mayer, A.E., Spear, P.M., Van Wyk, J.A., and Woods, G.S. (1994) Infrared absorption by the single nitrogen and A defect centres in diamond. Philosophical Magazine, B 69, 1141-1147.

Lawson, S.C., Fisherd, D., Hunt, D.C., and Newton, M.E. (1998) On the existence of positively charged single-substitutional nitrogen in diamond. Journal of Physics: Condensed Matter, 10, 6171-6180.

Lord, O.T., Walter, M.J., Dasgupta, R., Walker, D., and Clark, S.M., (2009) Melting in the Fe-C system to 70 GPa. Earth and Planetary Science Letters, 284, 157–167.

Luth, R.W. (2014) Volatiles in Earth's mantle. In Treatise on Geochemistry 3.9, 355-391. Elsevier, Oxford.

Marty, B. (2012) The origins and concentrations of water, carbon, nitrogen and noble gases on Earth and Planetary Science Letters, 313-314, 56-66.

Always consult and cite the final, published document. See http:/www.minsocam.org or GeoscienceWorld

Ohtani, E., and Maeda, M. (2001). Density of basaltic melt at high pressure and stability of the melt at the base of the lower mantle. Earth and Planetary Science Letters, 193(1-2), 69-75.

Pal'yanov, Y., Borzdov, Y., Kupriyanov, I., Gusev, V., Khokhryakov, A., and Sokol, A. (2001) High-pressure synthesis and characterization of diamond from a sulfur–carbon system. Diamond and related materials, 10(12), 2145-2152.

Palyanov, Y.N., Borzdov, Y.M., Khokhryakov, A.F., Kupriyanov, I.N., and Sobolev, N.V. (2006) Sulfide melts–graphite interaction at HPHT conditions: Implications for diamond genesis. Earth and Planetary Science Letters, 250(1-2), 269-280.

Palyanov, Y.N. and Sokol, A.G. (2009) The effect of composition of mantle fluids/melts on diamond formation processes. Lithos, 112, 690-700.

Palyanov, Yu.N., Borzdov, Yu.M., Khokhryakov, A.F., Kupriyanov, I.N., and Sokol, A.G. (2010) Effect of nitrogen impurity on diamond crystal growth processes. Crystal Growth & Design, 10, 3169–3175.

Palyanov, Yu.N., Bataleva, Y.V., Sokol, A.G., Borzdov, Y.M., Kupriyanov, I.N., Reutsky, V.N., and Sobolev, N.V. (2013) Mantle–slab interaction and redox mechanism of diamond formation. Proceedings of the National Academy of Sciences of the USA, 110. 20408-20413.

Roskosz, M., Bouhifd, M.A., Jephcoat, A.P., Marty, B., and Mysen, B.O. (2013) Nitrogen solubility in molten metal and silicate at high pressure and temperature. Geochimica et Cosmochimica Acta, 121, 15-28.

Smith, E.M., and Kopylova, M.G. (2014) Implications of metallic iron for diamonds and nitrogen in the sub-lithospheric mantle. Canadian Journal of Earth Sciences, 51, 510–516.

Sokol, A.G., Borzdov, Yu.M., Palyanov, Yu.N., Khokhryakov, A.F. (2015) High-temperature calibration of a multi-anvil high-pressure apparatus. High Pressure Research, 35, 139–147.

Sokol, A.G., Kruk, A.N., Seryotkin, Y.V., Korablin, A.A., and Palyanov, Y.N. (2017) Physics of the Earth and Planetary Interiors, 265, 43–53.

Always consult and cite the final, published document. See http:/www.minsocam.org or GeoscienceWorld

Sokol, A.G., Tomilenko, A.A., Bul'bak, T.A., Kruk, A.N., Zaikin, P.A., Sokol, I.A., Seryotkin, Y.V., and Palyanov, Y.N. (2018) Contributions to Mineralogy and Petrology, 173, 47.

Speelmanns, I.M., Schmidt, M.W., and Liebske, C. (2018). Nitrogen solubility in core materials. Geophysical Research Letters 45(15), 7434-7443.

Speelmanns, I.M., Schmidt, M.W., and Liebske, C. (2019). The almost lithophile character of nitrogen during core formation. Earth and Planetary Science Letters 510, 186-197.

Sugiura, N. (1998) Ion probe measurements of carbon and nitrogen in iron meteorites. Meteoritics & Planetary Science, 33(3), 393–409. https://doi.org/10.1111/j.1945-5100.1998.tb01645.x

Sun, S., Jia, X., Yan, B., Wang, F., Li, Y., Chen, N., and Ma, H. A. (2014) Synergistic effect of nitrogen and hydrogen on diamond crystal growth at high pressure and high temperature. Diamond and Related Materials, 42, 21-27.

Yu, R.Z., Ma, H.A., Liang, Z.Z., Liu, W.Q., Zheng, Y.J., Jia ,X. (2008) HPHT synthesis of diamond with high concentration nitrogen using powder catalyst with additive $Ba(N_3)_2$. Diamond and Related Materials, 17, 180-184.

Zhang, Y., Zang, C., Ma, H., Liang, Z., Zhou, L., Li, S., and Jia, X. (2008) HPHT synthesis of large single crystal diamond doped with high nitrogen concentration. Diamond and Related Materials, 17, 209–211.

FIGURE CAPTIONS

Fig. 1. Phases of quenched melt. a, b: dendritic crystals obtained by quenching of S-free C-saturated N-rich iron melt, sample 2005_2_2 (7.8 GPa and 1600°C), images of SEM (a) and optical microscopy after etching (b); c: dendritic crystals obtained by quenching of C-saturated N-

Always consult and cite the final, published document. See http:/www.minsocam.org or GeoscienceWorld

rich iron melt with 1 wt.% S, sample 1734_1_1 (5.5 GPa and 1600°C), SEM; d: graphite formed on a cleavage plane of quenched metal melt, sample 1728_1_2 (5.5 GPa and 1600°C), SEM.

Fig. 2. Concentrations of nitrogen (a) and carbon (b) in a graphite-saturated liquid Fe_3N at different pressures and temperatures, in the presence/absence of sulfur.

Fig. 3. Solubility of nitrogen and carbon in a Fe alloy melt equilibrated with graphite and boron nitride at 5.5 GPa and 1600°C in the presence of sulfur.

Fig. 4. Solubility of carbon in a graphite-saturated iron melt as a function of nitrogen contents at 7.8 GPa and 1350°C (Sokol et al., 2017).

Fig. 5. SEM micrographs of synthesized diamonds and boron nitride. a: aggregate of diamond crystals synthesized at 1600°C, a fragment; b, c: octahedral (b) and cyclic twin (c) diamonds synthesized at 1800°C; d: boron nitride tetrahedra on the {111} face of diamond.

Fig. 6. A representative FTIR spectrum of diamond crystals synthesized at 1600°C. Dashed curve is a reference spectrum of type IIa diamond shown for comparison.

Fig. 7. Representative FTIR spectra of diamond crystals synthesized at 1800°C. Inset shows one-phonone region for spectrum (a) together with a reference absorption spectrum of N+ defects.

Always consult and cite the final, published document. See http:/www.minsocam.org or GeoscienceWorld

Fig. 8. N content in a C-saturated Fe_3N melt as a function of pressure. N solubility in an iron melt at P_{N2}=0.1 MPa (Bouchard and Bale, 1995) is shown for comparison. Grey line is calculated N saturation limit from Speelmanns et al. (2018).

Fig. 9. N (a) and C (b) contents in a C-saturated in Fe alloy melt at 5.5-7.8 GPa and 1600-1800°C as a function of S content. Error bars are absent if they are smaller than the symbol size.

Supplementary Fig. 1. Contents of C (a) and N (b) in quenched melts determined using a *Jeol JXA-8100* microanalyzer (EPMA) and *Carlo Erba-1106 CHN* and *Euro EA 3000 CHNS* analyzers, compared.

Supplementary Fig. 2. Contents of S in quenched melts determined using a *JXA-8100* microanalyser (EPMA) and a *Euro EA 3000 CHNS* analyzer, compared.

Always consult and cite the final, published document. See http:/www.minsocam.org or GeoscienceWorld

Table 1. Run conditions in the Fe-C-N-S system, phase compositions of run products, and concentrations of C, N, S and B in quenched melts

Run#	Starting composition (wt.%)			Container	P (GPa)	T (°C)	Duration (min.)	Phase composition	Quenched liquid (wt.%)			
	Fe	S	N						C	N	S	B (ppm)
1728_1_2	92.9	-	7.1	Gr*	5.5	1600	60	Gr+L_q	3.9	6.6	n. a.	n. a.
1728_1_3	92.9	-	7.1	Gr	5.5	1600	60	Gr+L_q	3.6	6.5	n. a.	n. a.
1816_2_1	92.9	-	7.1	Gr	7.8	1450	60	Gr+L_q	2.5	6.2	n. a.	n. a.
1816_2_2	92.9	-	7.1	Gr	7.8	1450	60	Gr+L_q	1.4	8.8	n. a.	n. a.
2005_2_2	92.9	-	7.1	Gr	7.8	1600	30	Gr+L_q	2.3	6.9	n. a.	n. a.
2005_2_3	92.9	-	7.1	Gr	7.8	1600	30	Gr+L_q	2.4	7.6	n. a.	n. a.
2005_2_1	100	-	-	Gr	7.8	1600	30	Gr+L_q	6.2	n. d.	n. a.	n. a.
1743_1_1	90.9	2.0	7.1	Gr	5.5	1600	60	Gr+L_q	3.6	5.4	2.1	n. a.
1743_1_2	91.4	1.5	7.1	Gr	5.5	1600	60	Gr+L_q	3.5	4.3	1.4	n. a.
IN6*	92.9	-	7.7	Gr	7.0	1600	1200	Gr+Dm+L_q	2.3	7.8	n. a.	n. a.
IN7*	92.9	-	7.7	Gr	7.0	1550	1200	Gr+L_q	1.7	8.0	n. a.	n. a.
1734_1_1	91.4	1.5	7.1	BN+Gr	5.5	1600	60	BN+Gr+L_q	3.8	4.9	1.0	751
1734_1_2	90.9	2.0	7.1	BN+Gr	5.5	1600	60	BN+Gr+L_q	3.9	4.1	1.5	n. a.
2102_2_4	91.4	1.5	7.1	BN+Gr	5.5	1800	30	BN+Gr+L_q	4.4	4.0	0.9	504
1124_7_2	90.9	2.0	7.1	BN+Gr	5.5	1800	54	BN+Gr+L_q	4.3	4.7	1.4	n. a.
2106_2_1	91.4	1.5	7.1	BN+Gr	7.8	1600	60	BN+Gr+L_q	4.7	4.4	1.1	n. a.
2106_2_2	90.9	2.0	7.1	BN+Gr	7.8	1600	60	BN+Gr+Dm+L_q	4.6	4.3	1.1	n. a.
623_8_1	91.4	1.5	7.1	BN+Gr	7.8	1800	30	BN+Gr+Dm +L_q	5.2	3.3	1.5	n. a.
628_8_2	90.9	2.0	7.1	BN+Gr	7.8	1800	60	BN+Dm+L_q	3.9	5.4	1.7	776

Gr = graphite, Dm = diamond, BN = boron nitride, L_q = quenched liquid; n. a. is not analyzed, n.d. is not detected.
* samples of quenched liquid were obtained by Borzdov et al. (2002) but were not analyzed before for C and N contents; only growth of diamond on a seed was observed in run IN6.
The contents of C, N and S were determined using *Carlo Erba-1106 CHN* and *Euro EA 3000 CHNS* analyzers and are accurate within ±0.3 wt.%. The contents of B in metal alloy were determined on an *IRIS Advantage* atomic emission spectrometer, to an accuracy of 10 rel.%.

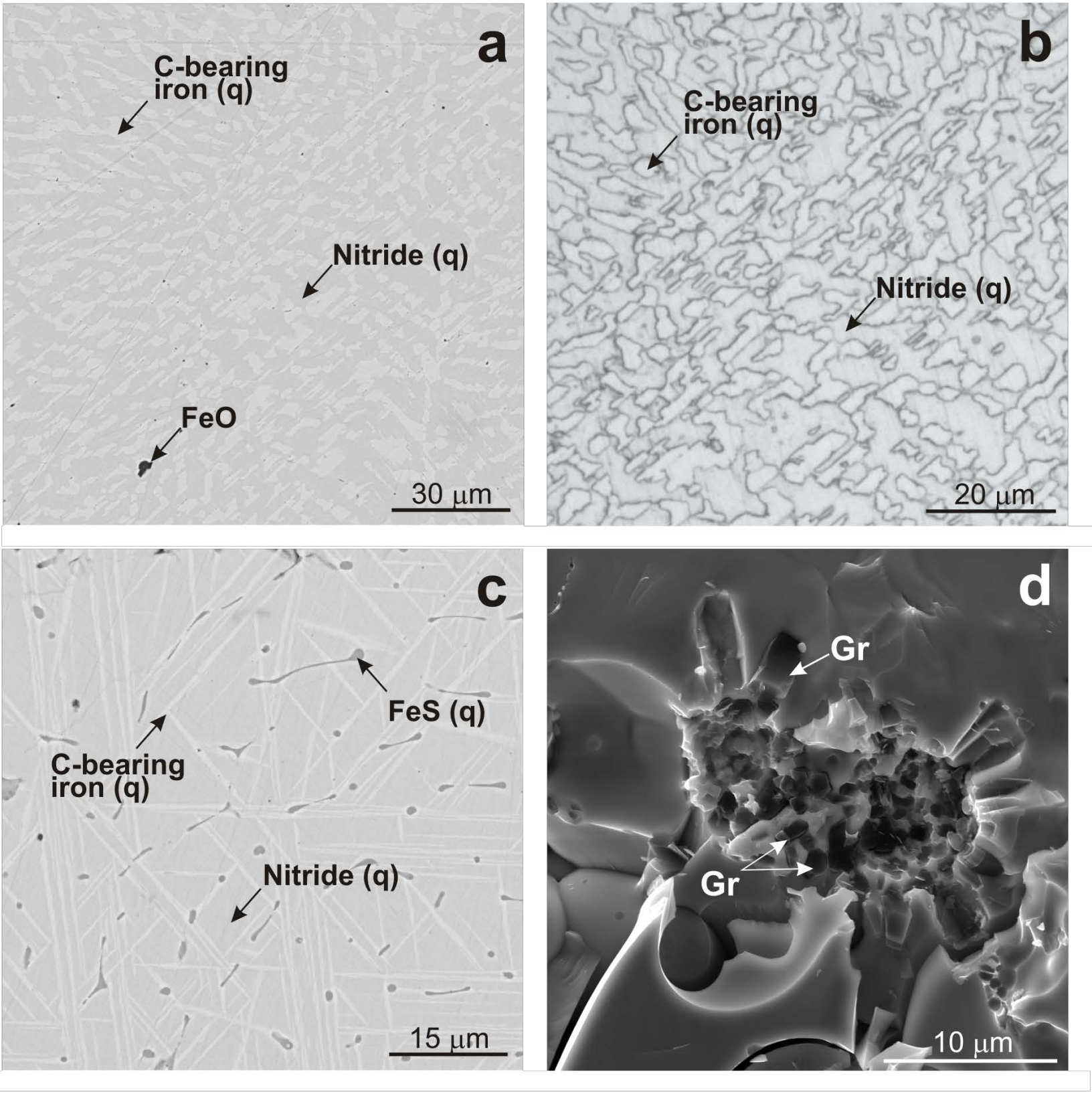
a
C-bearing iron (q)
Nitride (q)
FeO
30 μm
b
C-bearing iron (q)
Nitride (q)
20 μm
c
FeS (q)
C-bearing iron (q)
Nitride (q)
15 μm
d
Gr
Gr
10 μm

Fig.1

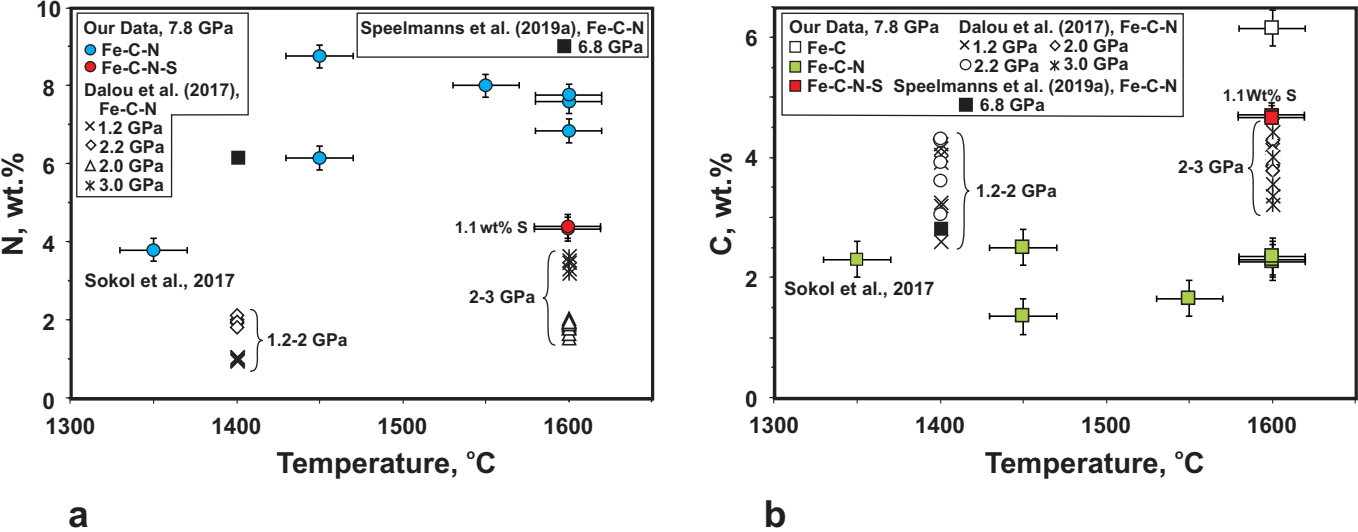
Our Data, 7.8 GPa
Fe-C-N
Fe-C-N-S
Dalou et al. (2017), Fe-C-N
1.2 GPa
2.2 GPa
2.0 GPa
3.0 GPa
Speelmanns et al. (2019a), Fe-C-N
6.8 GPa
1.1 wt% S
2-3 GPa
1.2-2 GPa
Sokol et al., 2017
N, wt.%
Temperature, °C
a
Our Data, 7.8 GPa
Fe-C
Fe-C-N
Fe-C-N-S
Dalou et al. (2017), Fe-C-N
1.2 GPa
2.0 GPa
2.2 GPa
3.0 GPa
Speelmanns et al. (2019a), Fe-C-N
6.8 GPa
1.1 Wt% S
2-3 GPa
1.2-2 GPa
Sokol et al., 2017
C, wt.%
Temperature, °C
b

Fig. 2

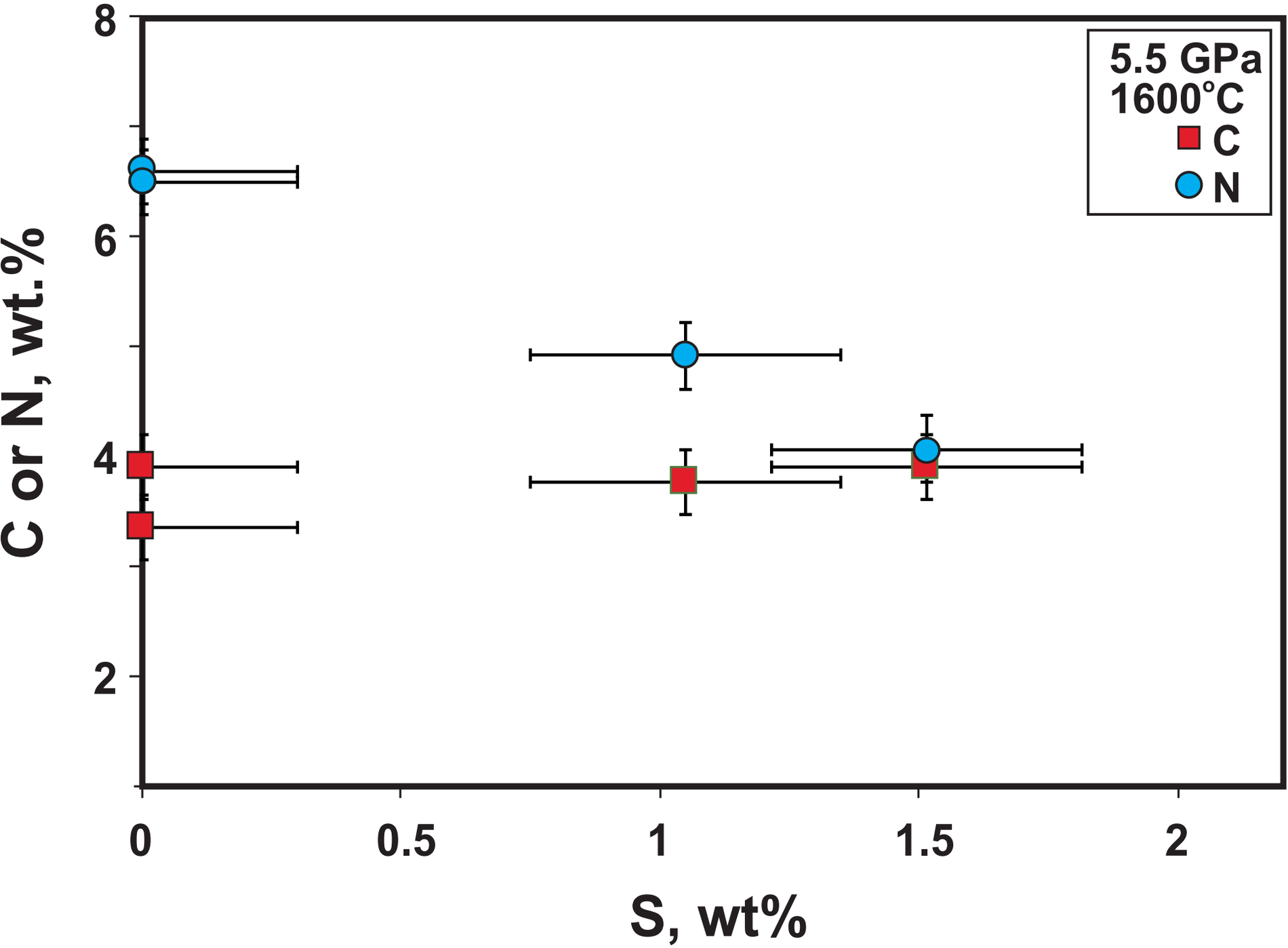

Fig. 3

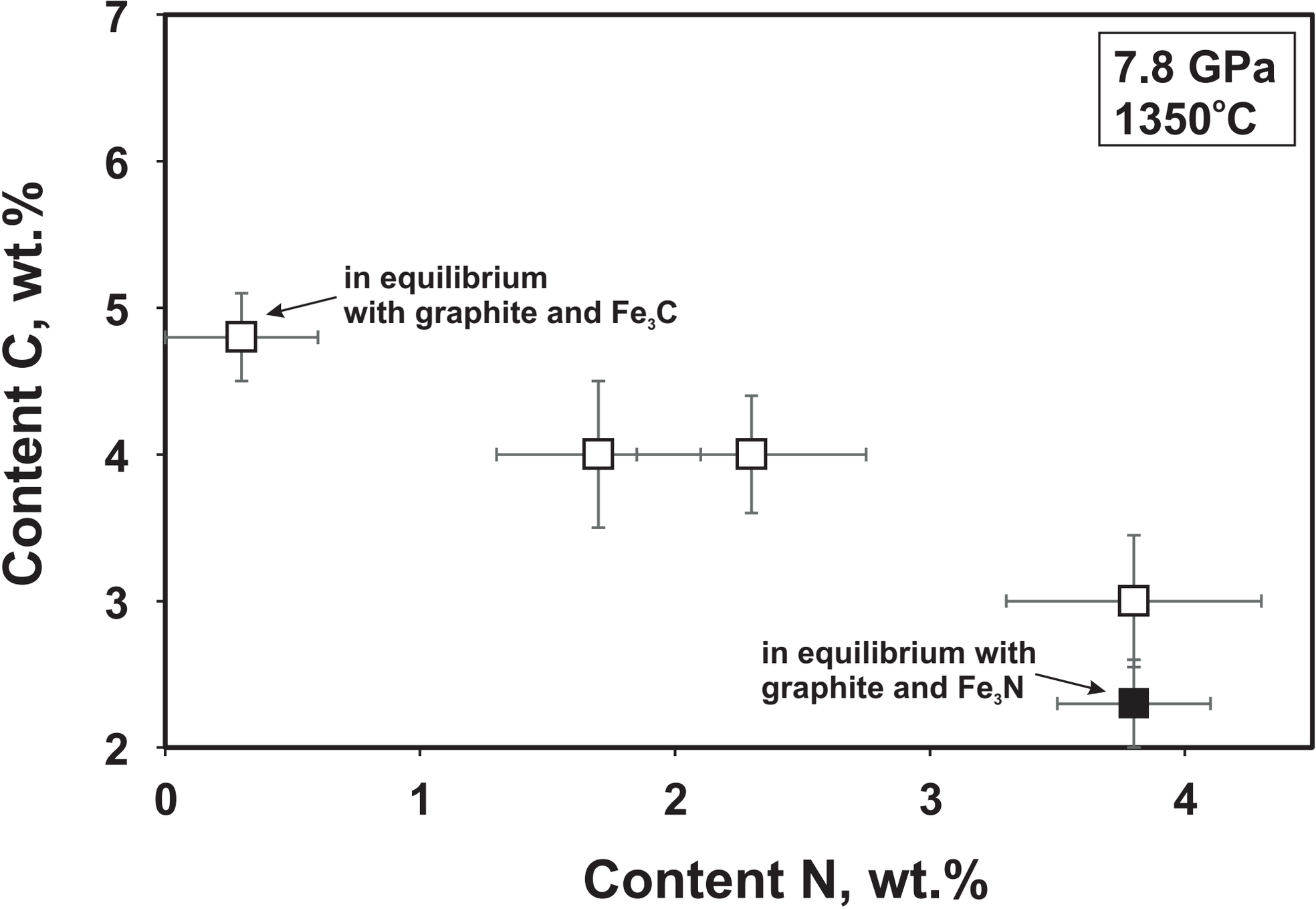
7.8 GPa
1350°C
in equilibrium
with graphite and Fe_3C
in equilibrium with
graphite and Fe_3N
Content C, wt.%
Content N, wt.%
7
6
5
4
3
2
0
1
2
3
4

Fig. 4

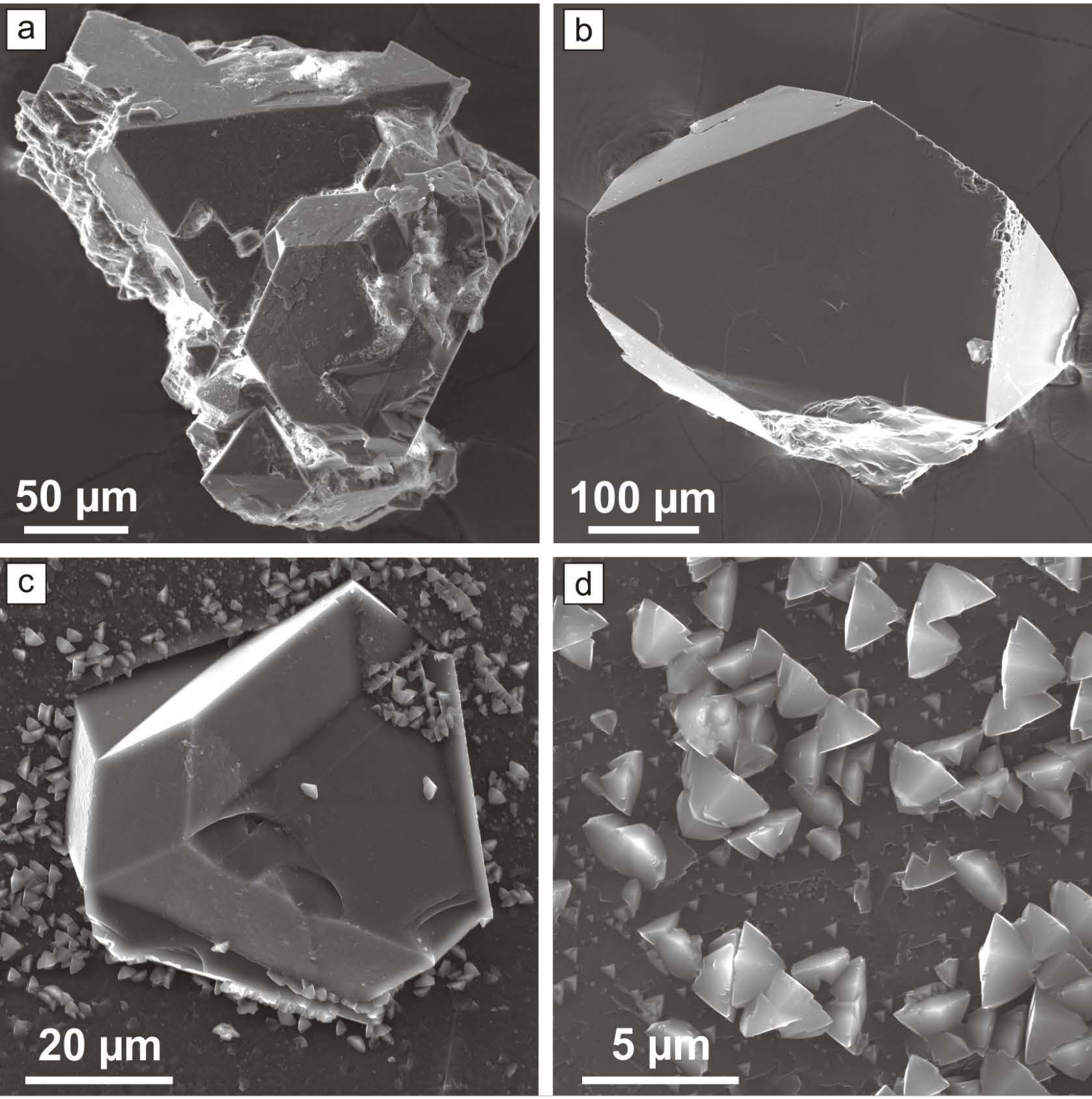

Fig. 5

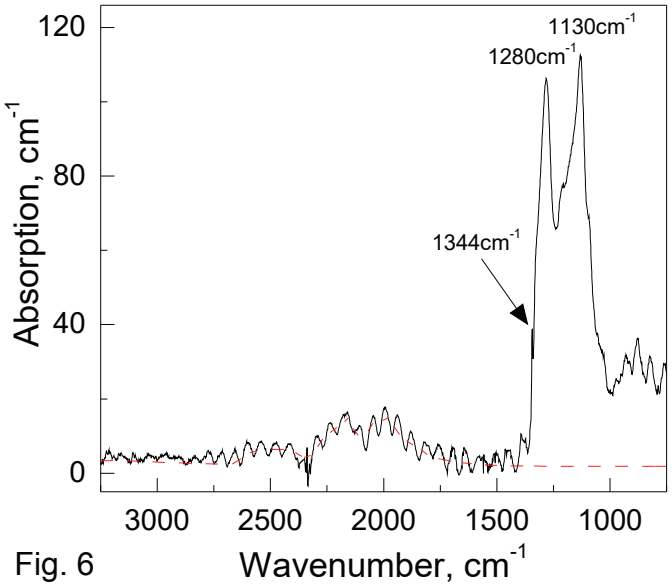
1130cm-1
1280cm-1
1344cm-1
120
80
40
0
Absorption, cm-1
3000
2500
2000
1500
1000
Wavenumber, cm-1

Fig. 6

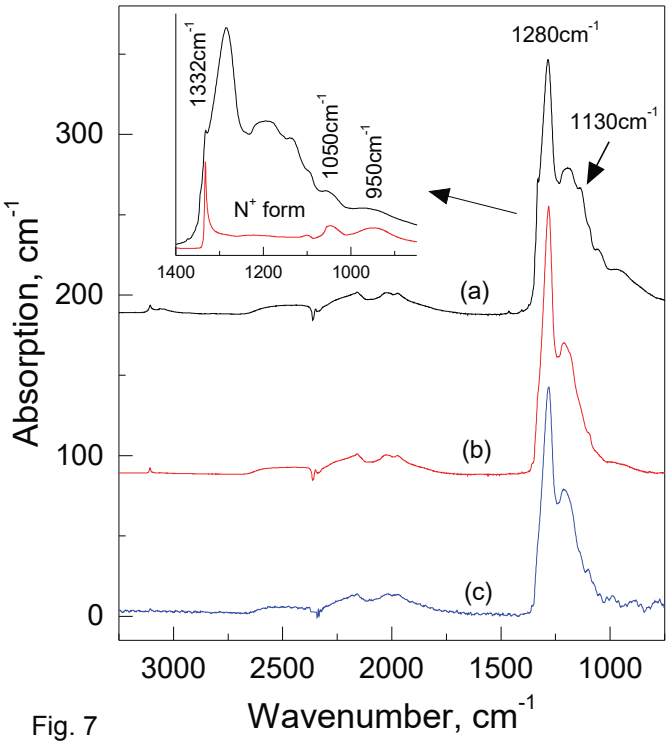
1280cm-1
1130cm-1
1332cm-1
1050cm-1
950cm-1
N+ form
1400
1200
1000
(a)
(b)
(c)
300
200
100
0
Absorption, cm-1
3000
2500
2000
1500
1000
Wavenumber, cm-1

Fig. 7

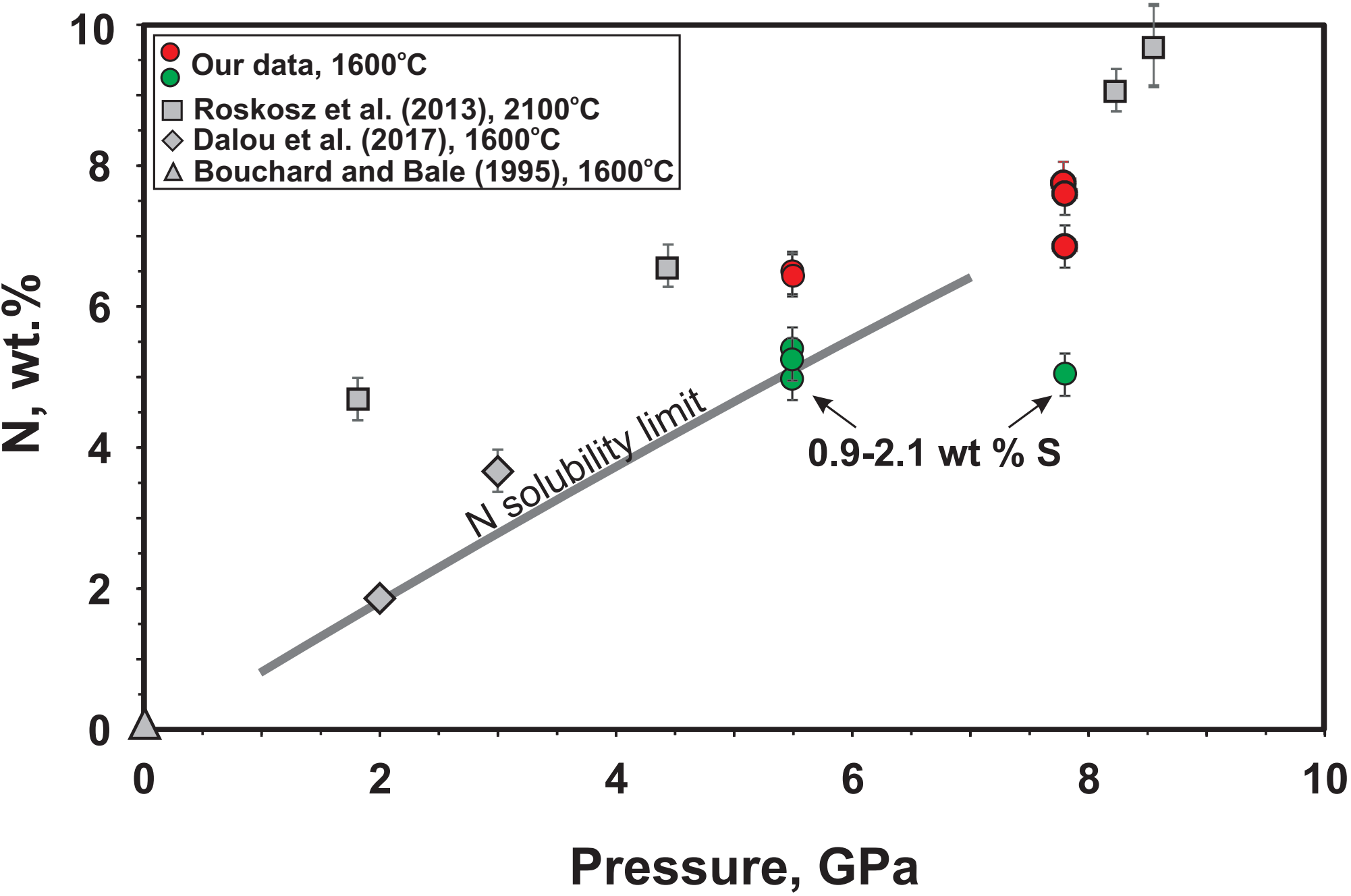
Our data, 1600°C
Roskosz et al. (2013), 2100°C
Dalou et al. (2017), 1600°C
Bouchard and Bale (1995), 1600°C
N solubility limit
0.9-2.1 wt % S
N, wt.%
Pressure, GPa
0
2
4
6
8
10

Fig. 8

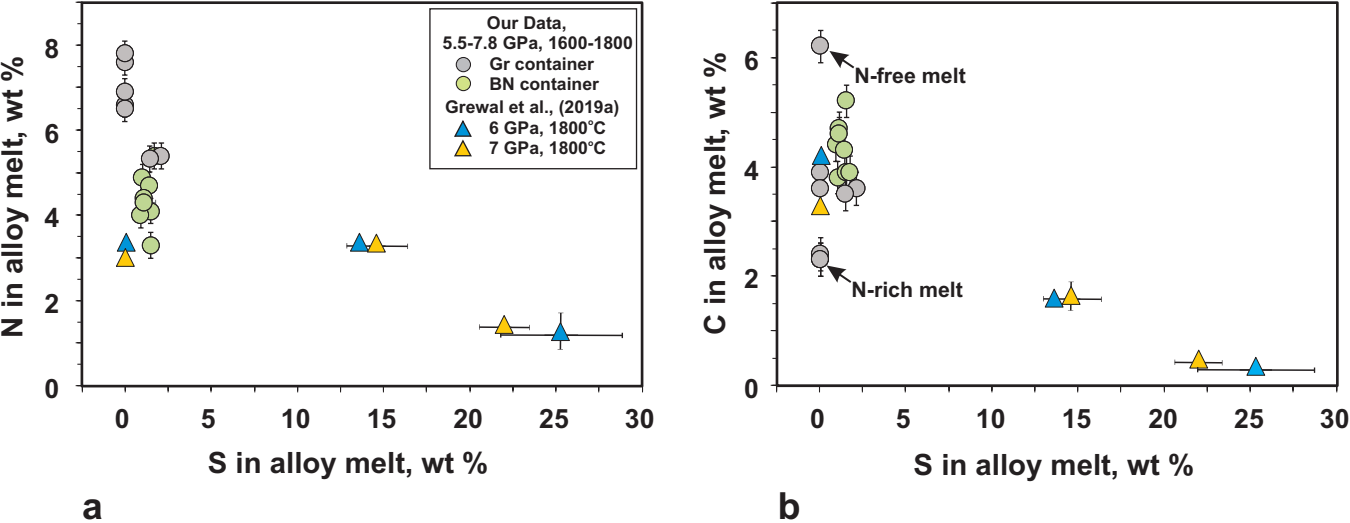
Our Data,
5.5-7.8 GPa, 1600-1800
Gr container
BN container
Grewal et al., (2019a)
6 GPa, 1800°C
7 GPa, 1800°C
N in alloy melt, wt %
S in alloy melt, wt %
a
N-free melt
N-rich melt
C in alloy melt, wt %
S in alloy melt, wt %
b

Fig. 9